

Simultaneous X-Ray and TeV Gamma-Ray Observations of the TeV Blazar Markarian 421 during February and May 2000

H. Krawczynski^{1,2,11}, R. Sambruna³, A. Kohnle², P.S. Coppi¹,

The HEGRA Collaboration: F. Aharonian², A. Akhperjanian⁹, J. Barrio^{4,5}, K. Bernlöhr²,
H. Börsch⁷, H. Bojahr⁸, O. Bolz², J. Contreras⁴, J. Cortina⁴, S. Denninghoff⁴, V. Fonseca⁵,
J. Gonzalez⁵, N. Götting⁶, G. Heinzelmann⁶, G. Hermann², A. Heusler², W. Hofmann²,
D. Horns², A. Ibarra⁵, I. Jung², R. Kankanyan², M. Kestel⁴, J. Kettler², A. Konopelko²,
H. Kornmeyer⁴, D. Kranich⁴, H. Lampeitl², E. Lorenz⁴, F. Lucarelli⁵, N. Magnussen⁸, O. Mang⁷,
H. Meyer⁸, R. Mirzoyan⁴, A. Moralejo⁵, L. Padilla⁵, M. Panter², R. Plaga⁵,
A. Plyasheshnikov^{2,10}, G. Pühlhofer², G. Rauterberg⁷, A. Röhring⁶, W. Rhode⁸, G. Rowell²,
V. Sahakian⁹, M. Samorski⁷, M. Schilling⁷, F. Schröder⁸, M. Siems⁷, W. Stamm⁷,
M. Tluczykont⁶, H.J. Völk², C. A. Wiedner², W. Wittek⁴

ABSTRACT

In this paper we present the results of simultaneous observations of the TeV blazar Markarian 421 (Mrk 421) at X-ray and TeV gamma-ray energies with the *Rossi X-Ray Timing Explorer (RXTE)* and the stereoscopic Cherenkov Telescope system of the HEGRA (High Energy Gamma Ray Astronomy) experiment, respectively. The source was monitored from February 2nd to February 16th and from May 3rd to May 8th, 2000.

¹Yale University, P.O. Box 208101, New Haven, CT 06520-8101, USA

²Max-Planck-Institut für Kernphysik, Postfach 103980, D-69029 Heidelberg, Germany

³George Mason University, 4400 University Drive, M/S 3F3, Fairfax, VA 22030, USA

⁴Max-Planck-Institut für Physik, Föhringer Ring 6, D-80805 München, Germany

⁵Universidad Complutense, Facultad de Ciencias Físicas, Ciudad Universitaria, E-28040 Madrid, Spain

⁶Universität Hamburg, II. Institut für Experimentalphysik, Luruper Chaussee 149, D-22761 Hamburg, Germany

⁷Universität Kiel, Institut für Experimentelle und Angewandte Physik, Leibnizstraße 15-19, D-24118 Kiel, Germany

⁸Universität Wuppertal, Fachbereich Physik, Gaußstr.20, D-42097 Wuppertal, Germany

⁹Yerevan Physics Institute, Alikhanian Br. 2, 375036 Yerevan, Armenia

¹⁰On leave from Altai State University, Dimitrov Street 66, 656099 Barnaul, Russia

¹¹Corresponding author, email krawcz@astro.yale.edu

In both energy bands several flares with very rapid flux variability were observed. In the X-ray band, the flux increased and decreased with e-folding times as short as about 5 hrs. The 3-20 keV photon index varied between values of 2.2 and 2.9. For 5 pointings the data shows statistically significant evidence for spectral curvature. The photon index varied substantially on very short time scales: on February 11th it hardened within 1.6 hrs by $\Delta\Gamma = 0.18$ and on February 14th it softened within 1.6 hrs by $\Delta\Gamma = 0.2$. The TeV observations of February 7th/8th showed statistically significant evidence for substantial TeV flux variability on 30 min time scale. The TeV energy spectrum averaged over all the observations of the campaign shows a similar steep slope as in earlier HEGRA observations: $dN/dE = N_0 \cdot (E/1 \text{ TeV})^{-\Gamma}$ with $N_0 = (25 \pm 1_{\text{stat}}) \cdot 10^{-12}$ photons $\text{cm}^{-2} \text{ s}^{-1} \text{ TeV}^{-1}$ and $\Gamma = 2.94 \pm 0.06_{\text{stat}}$. Within statistical errors no evidence for a curvature of the TeV energy spectrum is found. We show the results of modeling the data with a time dependent homogeneous Synchrotron Self-Compton (SSC) model. The X-ray and TeV gamma-ray emission strengths and energy spectra together with the rapid flux variability strongly suggest that the emission volume is approaching the observer with a Doppler factor of 50 or higher. The different flux variability time scales observed at X-rays and TeV Gamma-rays indicate that a more detailed analysis will require inhomogeneous models with several emission zones.

Subject headings: galaxies: BL Lacertae objects: individual (Mrk 421) — galaxies: jets — gamma rays: observations

1. Introduction

Since its early detection as a source of TeV gamma-rays (Punch et al. 1992; Petry et al. 1996) the BL Lac object Mrk 421 ($z = 0.031$) has been subject to very intensive studies throughout the electromagnetic spectrum. The study of this extreme gamma-ray loud blazar promises to elucidate the origin of jets of Active Galactic Nuclei (AGNs). Furthermore, the source is a laboratory for performing time resolved studies of the processes of particle acceleration and cooling. With a luminosity per solid angle of about $10^{44} \text{ erg s}^{-1} \text{ sr}^{-1}$ Mrk 421 is clearly a low-luminosity blazar. Nevertheless, the central black hole is estimated to be rather massive: Gorham et al. (1999) estimate a mass of between $1.8 \cdot 10^8$ and $3.6 \cdot 10^9$ solar masses.

Mrk 421 has intensively been studied at X-ray energies. Schubnell (1996) used the pointed X-ray telescopes on board of the *RXTE* satellite to monitor the source over a time period of 17 days. The 2-10 keV flux varied throughout the campaign by a factor of 10, while the photon index showed values between 2.3 to 3.4. Very detailed observation with integration times of several days have been carried through with the BeppoSAX instruments during the year 1997 and 1998 (Guainizzi et al. 1999; Maliza et al. 2000; Fossati et al. 2000a-b). Photon statistics limited the range in which

the spectrum could be determined to between 0.1 keV and ~ 15 keV. While single power law and broken power law fits did not describe the data satisfactorily, a model of the form $F(E) = K E^{\alpha_1} [1 + (E/E_b)^f]^{(\alpha_1 - \alpha_2)/f}$ incorporating continuous curvature resulted in statistically acceptable fits to the data (Fossati et al. 2000b). The Spectral Energy Distribution (SED) was found to peak in the energy range between 0.1 keV and 1.1 keV, or below 0.1 keV outside the energy range covered by the observations. The spectral slope around 5 keV was described by photon indices between 2.5 and 3.2.

At TeV energies Mrk 421 shows rapid flux variability on time scales down to a fraction of an hour (Gaidos et al. 1996). Within statistical errors the Mrk 421 energy spectra measured so far are consistent with pure power law spectra. The Whipple collaboration reported 260 GeV - 10 TeV photon indices of $2.54 \pm 0.04_{\text{stat}} \pm 0.1_{\text{syst}}$ and $2.45 \pm 0.1_{\text{stat}} \pm 0.1_{\text{syst}}$ for two very strong flares measured on May 7th and May 16th, 1996 with integral fluxes above a threshold energy of 350 GeV of 7.4 and 2.8 Crab units, respectively (Krennrich et al. 1999). The HEGRA collaboration reported steeper 0.5-5 TeV photon indices during several medium strong flares during 1997 and 1998 (between 1 and 2 Crab units above 1 TeV) without statistically significant evidence for a departure from the 1997–1998 mean index of $3.09 \pm 0.07_{\text{stat}} \pm 0.1_{\text{syst}}$ (Aharonian et al. 1999c).

The broadband flux variability was studied in several intensive observation campaigns and led to the discovery of pronounced TeV gamma-ray / X-ray flux correlations (Buckley et al. 1996; Takahashi et al. 1996). Recently, Takahashi et al. (2000) combined the results of intensive UV and X-ray observations performed with EUVE, BeppoSAX, and ASCA in April, 1998 with the TeV lightcurves measured with the CAT, HEGRA, and Whipple Cherenkov telescopes. The UV/X-ray flux showed “quasi-periodic” oscillations with a period of approximately 1/2 day and seemed to be well correlated with the TeV flux.

After observations in early February, 2000 with the HEGRA Cherenkov telescopes and the All Sky Monitor on board the *RXTE* satellite showed an increased TeV gamma-ray and X-ray activity of the source at a flux level comparable to the flux of the Crab Nebula, we asked the *RXTE* GOF to use a fraction of *RXTE* AO5 time, originally intended for monitoring Mrk 501, to observe the more active source Mrk 421.

In this paper we present the results of the coordinated X-ray (*RXTE*) and TeV gamma-ray (HEGRA) observations performed from February 2nd–16th, 2000 and from May 3rd–8th, 2000. The rest of the paper is structured as follows. In Sect. 2 we describe the X-ray and TeV gamma-ray data samples and data reduction and in Sect. 3 we present the observational results, i.e. the X-ray and TeV gamma-ray lightcurves, the flux correlation properties, the search for the shortest time scales of flux and spectral variability, and the X-ray and TeV energy spectra. In Sect. 4 we discuss the observational results in the framework of Synchrotron Self-Compton (SSC) models.

2. X-ray and TeV Gamma-Ray Data Sets and Data Reduction

2.1. X-Ray Data

The X-ray analysis described in the following is based on the 3-20 keV data from the Proportional Counter Array (PCA; Jahoda et al. 1996) on board the *RXTE* satellite. We did not use the 15–250 keV data from the High-Energy X-ray Timing Experiment (Rothschild et al. 1998) due to poor signal to noise ratio. Standard-2 mode PCA data gathered with the top layer of the operational PCUs (Proportional Counter Units) were analyzed. The number of PCUs operational during a pointing varied between 2 and 5. After applying the standard screening criteria, the net exposure in each Good Time Interval ranged from 16 secs to 3.15 ksecs (see Table 2). Spectra and lightcurves were extracted with FT00LSv5.0. Background models were generated with the tool `pcabackest`, based on the *RXTE* GOF calibration files for a “faint” source (less than 40 counts/sec/PCU). Response matrices for the PCA data were created with the script `pcarspv.2.43`. The spectral analysis was performed with the XSPECv.11.0.1 package. A constant neutral hydrogen column density of $2 \cdot 10^{20} \text{ cm}^{-2}$ was chosen, a value which lies close to the 21 cm line HI result of $1.6 \cdot 10^{20} \text{ cm}^{-2}$ (Dickey & Lockman 1990) and the BeppoSAX spectral absorption result of between $1.7 \cdot 10^{20} \text{ cm}^{-2}$ and $3.8 \cdot 10^{20} \text{ cm}^{-2}$ (Fossati et al. 2000b). Since the analysis is restricted to the energy region above 3 keV the chosen hydrogen column density has only a very minor influence on the estimated model parameters. The majority of measurements were satisfactorily described with single power law models; for days with long integration times and high count rates single power law models did not describe the data satisfactorily and we fitted broken power-law models. The quoted uncertainties on the spectral parameters are on the 67% confidence level ($\Delta\chi^2=1$) for the parameters of interest.

2.2. TeV Gamma-Ray Data

The TeV gamma-ray analysis presented in this paper is based on observations with the HEGRA Cherenkov telescope system (Konopelko et al. 1999) located on the Roque de los Muchachos on the Canary Island of La Palma (lat. 28.8° N, long. 17.9° W, 2200 m a.s.l.). The observations comprise a total of 61 hrs of best quality data. The analysis tools, the procedure of data cleaning and fine tuning of the Monte Carlo simulations, and the estimate of the systematic errors on the differential γ -ray energy spectra were discussed in detail by Aharonian et al. (1999a,b). The analysis uses the standard “loose” γ /hadron separation cuts which minimize systematic errors on flux and spectral estimates rather than yielding the optimal signal-to-noise ratio. A software requirement of two triggered Cherenkov Telescopes within 200 m from the shower axis, each with more than 40 photoelectrons per image and a “distance” parameter of smaller than 1.7° was used. Additionally, only events with a minimum stereo angle larger than 20° were admitted to the analysis. Integral

fluxes for certain energy intervals were obtained by integrating the differential energy spectra over the relevant energy region. By this means, the zenith angle dependence of the effective area has been corrected for and the results are largely independent of the assumed energy spectrum. For data runs during which the weather or the detector performance caused a Cosmic Ray detection rate deviating only slightly, i.e. less than 15% from the expectation value, the γ -ray detection rates and spectra were corrected accordingly. Spectra and fluxes above an energy threshold of 500 GeV were derived from the 43 hrs of data from zenith angles smaller than 30° . The search for variability within individual nights is based on the integral fluxes above 1 TeV and used all data with zenith angles up to 45° .

In the following, only statistical errors will be discussed. The systematic uncertainty in relative flux values is estimated to be smaller than 5%. Since the uncertainties in absolute fluxes are rather large, i.e. 30%, due to the 15% uncertainty in absolute energy scale, we will quote not only absolute flux values but also the flux strength compared to that from the Crab Nebula. The HEGRA measurement of the integral flux above 1 TeV from the Crab Nebula is $16.7 \cdot 10^{-12}$ photons $\text{cm}^{-2} \text{s}^{-1}$ (Aharonian et al. 2000). The systematic uncertainty on the 500 GeV – 5 TeV photon index is estimated to be 0.1.

3. Results

3.1. Lightcurves

The TeV gamma-ray and X-ray light curves as well as the 3-20 keV photon indices as function of time are shown in Figs. 1 and 2 for the February and May observations, respectively. The upper panels show the integral photon flux above 1 TeV determined on diurnal basis (solid symbols). The results from observations with zenith angles below and above 30° are shown separately to take advantage of the higher sensitivity of the Cherenkov Telescope System at zenith angles below $\sim 30^\circ$. The diurnal mean integral fluxes vary from values compatible with zero to $25 \cdot 10^{-12}$ photons $\text{cm}^{-2} \text{s}^{-1}$ (1.5 times the integral flux of the Crab Nebula above 1 TeV). Bad weather conditions resulted in only 2 days with good TeV data during the May *RXTE* observation campaign.

The center-panels of Figs. 1 and 2 show the 3-20 keV X-ray flux. During the February and May observations values of between $1.27 \cdot 10^{-10}$ and $1.02 \cdot 10^{-9}$ ergs $\text{cm}^{-2} \text{s}^{-1}$ were observed. The TeV gamma-ray and X-ray fluxes are correlated in the sense that both fluxes show their maximum emission strength around MJD 51581 (February 7th) and MJD 51586 (February 12th) and a minimum around MJD 51584 (February 10th). Note that the HEGRA observations had a mean duration of 1.8 h, considerably longer than the mean duration of 18 min of the *RXTE* observations. Furthermore, not all HEGRA and *RXTE* observations had an overlap in time. As discussed in the next subsection the TeV Gamma-ray fluxes substantially vary on time scales as short as a fraction

of an hour. A more detailed TeV gamma-ray/X-ray flux correlation analysis is hampered by the large statistical errors of the TeV flux estimates for adequately short integration times. This is shown by the open symbols in the upper panels of Figs. 1 and 2. Here, the HEGRA flux estimates have been computed with time bins of 15 min duration and only bins are shown which overlap with *RXTE* observations. Using 15 min time bins, the statistical errors on the TeV flux estimates are comparable to the amplitude of the flux variability.

The lower panels in Figs. 1 and 2 show the 3-20 keV photon indices. The photon indices vary from 2.9 for the days with the lowest flux level (MJD 51587-51590) to values of 2.2 for the days with the highest flux level (MJD 51581, 51667). The integral TeV gamma-ray fluxes and the results of the power-law fits to the X-ray data are summarized in Tables 1 and 2. For 5 observations with good photon statistics the power-law fits do not describe the X-ray data satisfactorily; broken power-law fits will be discussed below.

3.2. Shortest Variability Time Scales

We performed a search for the shortest TeV flux variability time scale based on a χ^2 -analysis of the integral fluxes above 1 TeV determined with a 15 min binning. The search revealed one night with significant flux variability. The integral fluxes above 1 TeV observed between MJD 51582.06 and MJD 51582.27 (February 8th) are shown in the upper panel of Fig. 3. Within 1 hr the TeV flux increases from a level consistent with zero to $(64 \pm 12_{\text{stat}}) \cdot 10^{-12}$ photons $\text{cm}^{-2} \text{s}^{-1}$ ($3.9 \pm 0.7_{\text{stat}}$ Crab units). A fit of a constant to the integral fluxes is rejected with a chance probability of $1.0 \cdot 10^{-5}$. Our observation of substantial TeV Gamma-ray flux variability on sub-hour time scale confirms the existence of substantial sub-hour flux variations reported for the strong May 7th, 1996 Mrk 421 flare (Gaidos et al. 1996).

The (2-5 TeV)/(1-2 TeV) hardness ratios are shown in the lower panel of Fig. 3. The hardness ratios have been computed with the 1-2 TeV and 2-5 TeV photon fluxes after correction for the (modest) zenith angle dependent variation of the effective area over the considered energy range (Aharonian et al. 1999a). For a TeV energy spectrum of photon index Γ the expected hardness ratio is then given by $r_{\text{exp}}(\Gamma) = (2^{-\Gamma+1} - 5^{-\Gamma+1}) / (1 - 2^{-\Gamma+1})$ for $\Gamma > 1$ and $\ln(5/2)/\ln(2)$ for $\Gamma = 1$. The values for $\Gamma = 1, 2, 3,$ and 4 are shown as lines in the lower panel of Fig. 3. The hardness ratios do not show evidence for spectral variability during the flare. A fit of a constant with a mean value of 0.23 gives a χ^2 value of 11.7 for 8 degrees of freedom corresponding to a probability of 16.5% for a higher value by chance. The data following MJD 51582.225 has been taken under zenith angles larger than 30° , where systematic errors start to be non-negligible. For these points (which do not enter strongly the χ^2 -value cited above) the 1-2 TeV flux is uncertain by about 50%; accordingly, the latest hardness ratio point has a systematic error comparable to the statistical one. Unfortunately, *RXTE* observations were only performed during the first 1.5 hrs

of the 4.8 hrs of HEGRA observations (see Fig. 3, upper panel) and did not cover the time of the strong TeV gamma-ray flare.

We analyzed the X-ray flux variability time scale by computing the e -folding times from the flux changes between observations: $\tau = \Delta t / \Delta \ln F(3 - 20 \text{ keV})$ with Δt the time difference between two observations and $\Delta \ln F(3 - 20 \text{ keV})$ the difference of the logarithms of the 3-20 keV fluxes. The shortest e -folding times are given in Table 3. Flux increases and decreases with e -folding times down to $\simeq 5.8$ hrs and $\simeq 4.1$ hrs have been found, respectively.

We searched for rapid spectral changes by analyzing the change of spectral indices between *RXTE* observations. The fastest spectral changes are listed in Table 4. The fastest spectral variability is characterized by changes in photon index of $\simeq 0.12/\text{hr}$. We found similarly rapid spectral hardening as softening: on MJD 51585 (February 11th) the spectrum hardened by 0.18 in 1.6 hrs and on MJD 51588 (February 14th) the spectrum softened by 0.2 in 1.6 hrs.

3.3. TeV Gamma-ray and X-ray Energy Spectra

In the energy range from 500 GeV to 5 TeV the time averaged spectrum of the February observations (MJD 51576 – MJD 51589) is well described by a pure power law model: $dN/dE = N_0 \cdot (E/1 \text{ TeV})^{-\Gamma}$ with $N_0 = (25 \pm 1_{\text{stat}})$ photons $\text{cm}^{-2} \text{ s}^{-1} \text{ TeV}^{-1}$ and $\Gamma = 2.94 \pm 0.06_{\text{stat}}$. The fit has a χ^2 -value of 15.6 for 7 degrees of freedom (chance probability 5%). In Table 5 we give the results of the power law fits for individual days for which the accuracy in the determined photon index is better than 0.3. The photon indices lie between 2.70 and 3.02 but the deviation from the mean index of 2.94 is statistically not significant. The large χ^2 -value of the spectrum of MJD 51582.0603 stems from two underpopulated bins centered at energies of 700 GeV and 4.35 TeV and indicates spectral softening with increasing energy. A more detailed discussion of the curvature of the TeV energy spectra which takes fully into account the systematic uncertainties is outside the scope of this paper and will be given in an upcoming paper in which the full year 2000 data set is included.

As shown in Table 2, a pure power law fit does not give an acceptable fit to the data (chance probability well below 1%) for 5 *RXTE* observations with good photon statistics. We find that broken power law models describe the data of these 5 pointings satisfactorily and the results of fits to the 3-25 keV data are given in Table 6. The estimated break energies lie in the range between 6.6 keV and 8 keV and the difference between the low and the high energy power law photon indices are about 0.2. Due to the limited energy coverage of our X-ray observations we did not fit the data with more complex models incorporating continuous spectral curvature. We investigated if the other *RXTE* data sets are consistent with a similar change in spectral index by fitting these data sets with a broken powerlaw model with a fixed break energy at 7.3 keV (the mean break

energy found for the data sets of Table 6). Indeed, all fits suggest spectral steepening and we find a median value of the change in spectral index of 0.16, very similar to the mean change in spectral index of 0.19 found for the data sets of Table 6.

4. Discussion

During our observation campaign, the X-ray photon index varied from values between 2.2 to 2.9. Cooling of a power law distribution of electrons changes the synchrotron spectral index by at most 0.5 (Kardashev 1962). Therefore, the observations clearly show that either the spectral index of accelerated particles is variable, or that we observe the cooling of electrons near the high energy cut-off of the particle acceleration process. The TeV gamma-ray/X-ray emission of Mrk 421 is commonly attributed to the SSC mechanism (see for alternative models Aharonian et al. 2000, and references therein) in which a population of high energy electrons emits synchrotron radiation at longer wavelengths and high energy photons from Inverse Compton (IC) processes of high energy electrons with lower energy synchrotron photons at shorter wavelengths.

Our initial modeling of the X-ray/TeV Gamma-ray data with the time dependent SSC code described by Coppi (1992) allows already some interesting conclusions which we will detail in the following. We focus on modeling the observations taken on an individual day, i.e., MJD 51581, where a large change in X-ray flux and spectrum had been observed and the TeV spectrum has been determined with reasonable statistical accuracy. We adopt a spherical emission volume of radius $R = 2.7 \cdot 10^{15}$ cm which satisfies the constraints from the observed flux variability $R \lesssim \delta_j c \Delta T_{\text{obs}} = 2.7 \cdot 10^{15}$ cm for a jet Doppler factor¹² $\delta_j = 50$ and flux variability time scale $\Delta T_{\text{obs}} = 30$ min. We assume a randomly oriented magnetic field of mean strength $B = 0.22$ G (in jet frame). For this magnetic field, electrons of Lorentz factor $\gamma_e = 1.8 \cdot 10^5$ which produce synchrotron radiation with maximum power per logarithmic energy band at energy $\varepsilon \approx (3/4\pi) \delta_j h e \langle \sin \theta \rangle B \gamma_e^2 (m_e c)^{-1} \approx 5$ keV (h is Planck's constant, e the electron charge, $\langle \sin \theta \rangle = \sqrt{2/3}$) have an observed radiative cooling time $t_s = [\frac{4}{3} \sigma_T c \delta_j \frac{B^2}{8\pi m_e c^2} \gamma_e]^{-1}$ (σ_T the Thomson cross section) of ≈ 30 min, comparable to the fastest variability time scale during the observation campaign. We inject a power law of accelerated electrons $q(\gamma_e, t) = \text{const} \cdot \gamma_e^{-p} \exp(-\gamma_e/\gamma_{\text{max}}(t))$ with $p = -2$ (the expected value for diffuse particle acceleration at strong shocks), and assume a Hubble constant of $H_0 = 60 \text{ km s}^{-1} \text{ Mpc}^{-1}$ and a deceleration parameter of $q_0 = 0.5$.

Following Mastichiadis & Kirk (1997) we model the temporal evolution of X-ray flux and spectrum by changing γ_{max} only. We use a damping term for the electron density inside the source

¹²The jet Doppler factor is defined as $\delta_j^{-1} = \Gamma(1 - \beta \cos(\theta))$, with Γ the bulk Lorentz factor, and β the bulk velocity in units of the speed of light of the emitting volume, respectively, and θ is the angle between jet axis and the line of sight as measured in the observer frame.

of $\partial n_e/\partial t \propto -n_e/t_{\text{esc}}$ with an escape time t_{esc} of 5 light crossing times. We use a minimum Lorentz factor of accelerated particles of $\gamma_{\text{min}} = m_{\text{P}}/m_e = 1836$ (ratio of proton to electron mass), above which diffusive shock acceleration is probable to work (Eilek & Hughes 1991). The results in the X-ray and TeV energy ranges do not depend strongly on the value of γ_{min} (as long as it is smaller than $\approx 10^4$) and the model does not need fine tuning of these parameters. Conversely, the emission strength in the infrared and optical bands do depend on the value of γ_{min} . A multiwavelength campaign with observations in these bands, together with X-ray and TeV Gamma-ray coverage would make it possible to assess this important parameter of particle acceleration theories.

The solid lines in Fig. 4 show the result of calculations where we modeled the relatively high flux level observed on MJD 51581 by changing γ_{max} from an initial value of $1.4 \cdot 10^5$ to a maximum value of $5.0 \cdot 10^5$. The model satisfactorily describes the X-ray flux and X-ray spectral index and the TeV flux. Note that the observational coverage is much too sparse to pin down the temporal evolution of the source. Very different choices of the temporal evolution of the maximum Lorentz factor of accelerated particles $\gamma_{\text{max}}(t)$ are able to describe the data, as shown e.g. by the dashed line in Fig. 4. Some properties of the SSC model calculations however do not depend strongly on the adopted hypothesis of what causes individual flares. In the following we will focus on these properties.

Figure 5 compares the observed Spectral Energy Distributions (SEDs) with the ones from the SSC model (“Model 1” shown by solid lines in Fig. 4). Given the constraints on the size of the emission volume from the observed flux variability, we did not achieve to fit the combined X-ray and TeV Gamma-ray data with jet Doppler factors substantially below 50. Lower Doppler factors resulted either in a strong overproduction of TeV Gamma-rays for small values of the mean magnetic field ($B \ll 0.22$ G), or in a too steep TeV energy spectrum for high values of the mean magnetic field ($B \gg 0.22$ G). Also a sharper high energy cut-off in the spectrum of accelerated particles did not reduce the IC photon yield substantially. Reducing the jet Doppler factor by using a minimum Lorentz factor of accelerated particles requires γ_{min} -values of several times 10^4 which is difficult to motivate theoretically. Taking into account extragalactic extinction would result in even higher Doppler factors since the effect is expected to steepen the observed TeV Gamma-ray spectrum while reducing the Gamma-ray flux around 1 TeV by a factor $\lesssim 2$ (Stecker & De Jager; Primack et al. 2001). Furthermore, external seed photons, neglected in our analysis, would result in an even higher model prediction of the emitted TeV Gamma-ray flux.

Our modeling differs from earlier work which indicated Doppler factors of about 15 (see e.g. Inoue & Takahara 1996, Mastichiadis & Kirk 1997, Takahashi et al. 2000) by one or several of the following reasons: we use a small emission volume (consistent with flux variability on 30 min time scale), a minimum Lorentz factor of accelerated electrons well below 10^4 , and snapshots of an evolving electron spectrum instead of steady state electron spectra. Since the cooling times of the electrons responsible for the X-ray and TeV Gamma-ray emission are comparable to the duration

of individual flares, steady state electron populations overestimate the extend to which electron spectra cool before, during, and after individual flares. Note that SSC models with Doppler factors of about 15 predict, in agreement with the results of our code, TeV energy spectra which are softer than the ones which have been observed so far (Inoue & Takahara (1996), Takahashi et al. (2000)).

For high Doppler factors, the energy density of relativistic electrons and that of the magnetic field are more comparable than for low Doppler factors (compare Inoue & Takahara 1996): for our choice of γ_{\min} and δ_j the energy density of relativistic particles is $u_e \approx 0.01 \text{ erg cm}^{-3}$ and that of the magnetic field is $u_B \approx 0.002 \text{ erg cm}^{-3}$. The model requires a modest minimum kinetic power (see e.g. Begelman et al. 1994) transported by the jet $L_j = \Gamma^2 (u_e + u_p + u_B) c r^2 \Delta\Omega$ of $\approx 4.25 \cdot 10^{43} \text{ erg s}^{-1}$. Here we assumed $\Gamma = 50$, a distance of the emission region from the central engine of $r = 10^{16} \text{ cm}$, and a solid angle subtended by the jet of $\Delta\Omega \approx 2\pi(1 - \cos(\Gamma^{-1})) = 1.26 \cdot 10^{-3} \text{ sr}$. Furthermore we assumed a factor of $\kappa = 1000$ more cold electrons than relativistic electrons (the density of relativistic electrons in our models is: $\approx 3 \text{ cm}^{-3}$) and an equal number of electrons and cold protons, giving a comoving energy density in cold protons of $u_p = 4.5 \cdot ((\kappa + 1)/1001) \text{ erg cm}^{-3}$.

In accordance with earlier observations (Gaidos et al. 1996; Takahashi et al. 1996; Maraschi et al. 1999; Fossati et al. 2000a) we find shorter flux variability at TeV energies than at X-ray energies with shortest e -folding times of $\approx 1 \text{ hr}$ at TeV energies and $\approx 5 \text{ hrs}$ at X-ray energies, respectively. This finding could naturally be explained in the framework of an inhomogeneous SSC model. If the region of particle acceleration is relatively small, an event of enhanced particle acceleration could result in a rapidly variable TeV Gamma-ray component originating from the vicinity of the acceleration region while the observed X-rays, dominated by the emission of particles of earlier acceleration events, could vary more slowly. If strong internal shocks accelerate the electrons, one indeed expects that the accelerated particles are bound to the downstream medium by the same scattering processes which enable particle acceleration. If the density of relativistic particles decreases downstream (due to particle diffusion or due to adiabatic expansion of the downstream plasma) the SSC mechanism then guarantees that the IC emissivity decreases faster than the synchrotron emissivity. Although the synchrotron emission of such a system has been discussed in the literature (see e.g. Heavens & Meisenheimer (1987), Kirk et al. (1998)), the consequences for the temporal evolution and correlation of the synchrotron and the IC components have not yet been studied. The upcoming Cherenkov telescope experiments CANGAROO III, H.E.S.S., MAGIC, and VERITAS with one order of magnitude higher sensitivity than present instruments will make it possible to test such inhomogeneous models, and to infer details about the geometry and dynamics of the radiating plasma. To “map” in this way the jet at its base in the very vicinity of the black hole is a very exciting prospect of Gamma-ray astronomy indeed.

Acknowledgments. We thank Jean Swank and the *RXTE* GOF for allowing us to use the *RXTE*

time for Mrk 421 observations. The support of the German ministry for Research and Technology BMBF and of the Spanish Research Council CYCIT is gratefully acknowledged. We thank the Instituto de Astrofísica de Canarias for the use of the site and for supplying excellent working conditions at La Palma. We gratefully acknowledge the technical support staff of the Heidelberg, Kiel, Munich, and Yerevan Institutes. Rita Sambruna is supported by NASA AOP grant NAG 5-27016.

REFERENCES

- Aharonian, F.A. 2000, *New A*, 5, 377
- Aharonian, F.A., Akhperjanian, A.G., Barrio, J.A., et al. 1999a, *A&A*, 342, 69
- Aharonian, F.A., Akhperjanian, A.G., Barrio, J.A., et al. 1999b, *A&A*, 349, 11
- Aharonian, F.A., Akhperjanian, A.G., Andronache, M., et al. 1999c, *A&A*, 350, 757
- Aharonian, F.A., Akhperjanian, A.G., Barrio, J.A., et al. 2000, *ApJ*, 539, 317
- Begelman, M.C., Rees, M.J., Sikora, M. 1994, *ApJ*, 429, L57
- Buckley, J.H., Akerlof, C.W., Biller, S., et al. 1996, *ApJ*, 472, L9
- Coppi, P.S. 1992, *MNRAS* 258, 657
- Dickey, J.M., Lockman, F.J. 1990, *Ann. Rev. Ast. Astr.* 28, 215
- Eilek, J.A., Hughes, P.A. 1991, In: “Beams and Jets in Astrophysics”, ed P.A. Hughes, Cambridge University Press
- Fossati, G., Celotti, A., Chiaberge, A., et al. 2000a, *ApJ*, 541, 153
- Fossati, G., Celotti, A., Chiaberge, A., et al. 2000b, *ApJ*, 541, 166
- Gaidos J.A., Akerlof C.W., Biller S.D., et al., 1996, *Nat* 383, 319
- Guainizzi, M., Vacanti, G., O’Flaherty, K.S., Palazzi, E., Parmar, A.N. 1999, *A&A*, 342,124
- Heavens, A.F., Meisenheimer, K. 1987, *MNRAS*, 225, 335
- Inoue, S., Takahara, F. 1996, *ApJ*, 463, 555
- Kardashev N.S., 1962, *Soviet Astronomy*, V. 6, N. 3, p. 317
- Kirk, J. G., Rieger, F. M., Mastichiadis, A. 1998, *A&A*, 333, 452
- Krawczynski, H., Coppi, P.S., Maccarone, M., et al. 2000, *A&A*, 353, 97
- Krennrich, F., Biller, S.D., Bond, I.H. et al. 1999, *ApJ*, 511, 149
- Macomb, D.J., Akerlof, C.W., Aller, H.D., et al. 1995, 449, L99
- Malizzia, A., Capalbi, M., Fiore, F., et al. 2000, *MNRAS*, 312, 123
- Maraschi, L., Fossati, G., Tavecchio, F., et al. 1999, *Astropart.Phys.*, 11, 189
- Mastichiadis, A., Kirk, J.G., 1997, *A&A*, 320, 19

- Petry, D., Bradbury, S. M., Konopelko, A., et al. 1996, A&A 311, L13
- Primack, J.R., Somerville R.S., Bullock J.S., Devriendt, J.E.G. 2000, In: Procs. of the International Symposium on Gamma-Ray Astronomy, Heidelberg, June 2000, eds F. Aharonian and H. Völk, AIP Conf. Proc
- Punch, M., Akerlof, C. W., Cawley, M. F., et al. 1992, Nat 358, 477
- Schubnell, M.S. 1996, AAS, 189, 3105
- Stecker, F.W., De Jager, O.C., 1998, A&A, 334, L85
- Takahashi, T., Tashiro, M., Madejski, G., et al., 1996, ApJ 470, L89
- Takahashi, T., Kataoke, G., Madejski, G., et al. 2000, ApJ, 542, L105

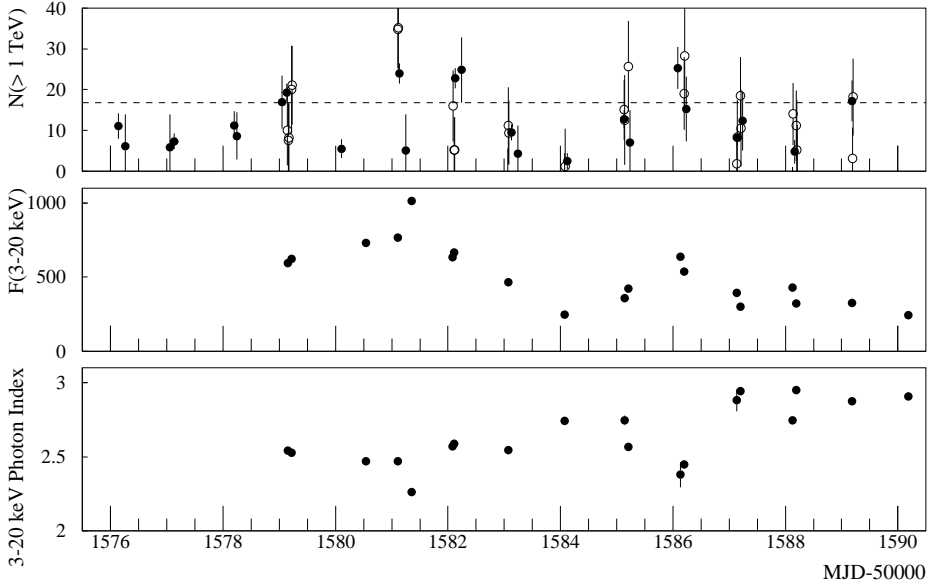


Fig. 1.— The TeV gamma-ray and X-ray results from February, 2000. The upper panel shows the integral flux above 1 TeV ($N(> 1 \text{ TeV})$) in units of $10^{-12} \text{ photons cm}^{-2} \text{ s}^{-1}$. The full symbols show the diurnal results separately for data from zenith angles below and above 30° , the open symbols show the flux as determined with 15 min bins for all bins which overlap with *RXTE* observations. The dashed line indicates the steady flux level of the Crab Nebula. The center-panel shows the 3-20 keV X-ray flux $F(3 - 20 \text{ keV})$ in units of $10^{-12} \text{ ergs cm}^{-2} \text{ s}^{-1}$. The lower panel shows the 3-20 keV photon index. MJD 51576 corresponds to February 2nd, 2000.

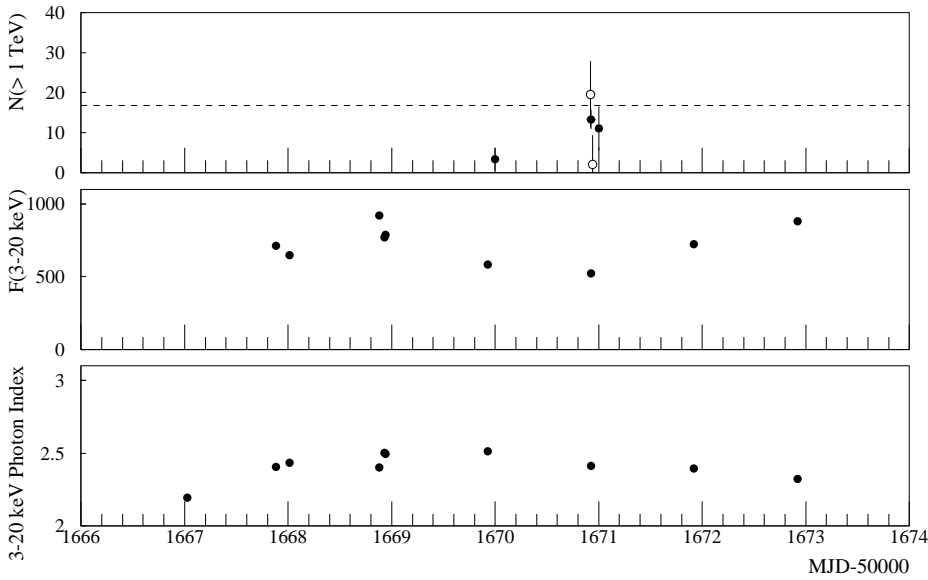


Fig. 2.— The TeV gamma-ray and X-ray results from May, 2000. The symbols and units are the same as in Fig. 1. MJD 51667 corresponds to May 3rd, 2000.

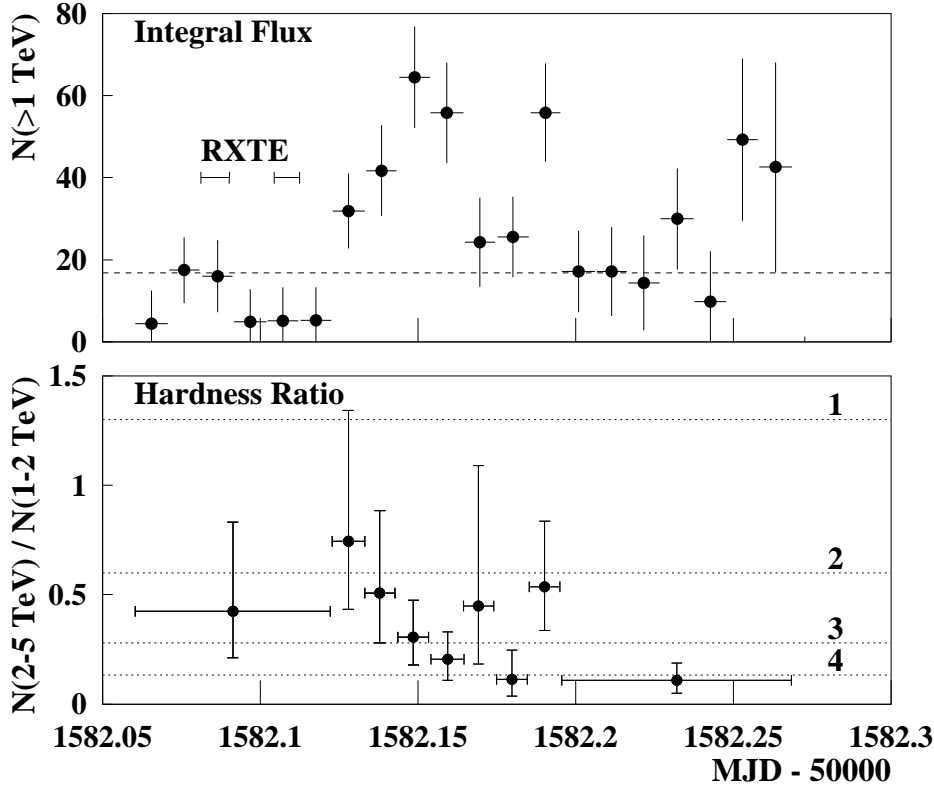


Fig. 3.— The TeV gamma-ray results from February 8th, 2000. The upper panel shows the integral flux above 1 TeV ($N(> 1 \text{ TeV})$) in units of $10^{-12} \text{ photons cm}^{-2} \text{ s}^{-1}$ with time bins of 15 min length. The dashed line indicates the steady flux level of the Crab Nebula and the 2 horizontal lines show the *RXTE* coverage. The lower panel shows the $N(2-5 \text{ TeV}) / N(1-2 \text{ TeV})$ hardness ratios (median values with 1 sigma confidence intervals). The dotted lines show the expected hardness ratios for photon indices of 1, 2, 3, and 4, as labelled. Statistical errors only, see text for systematic errors.

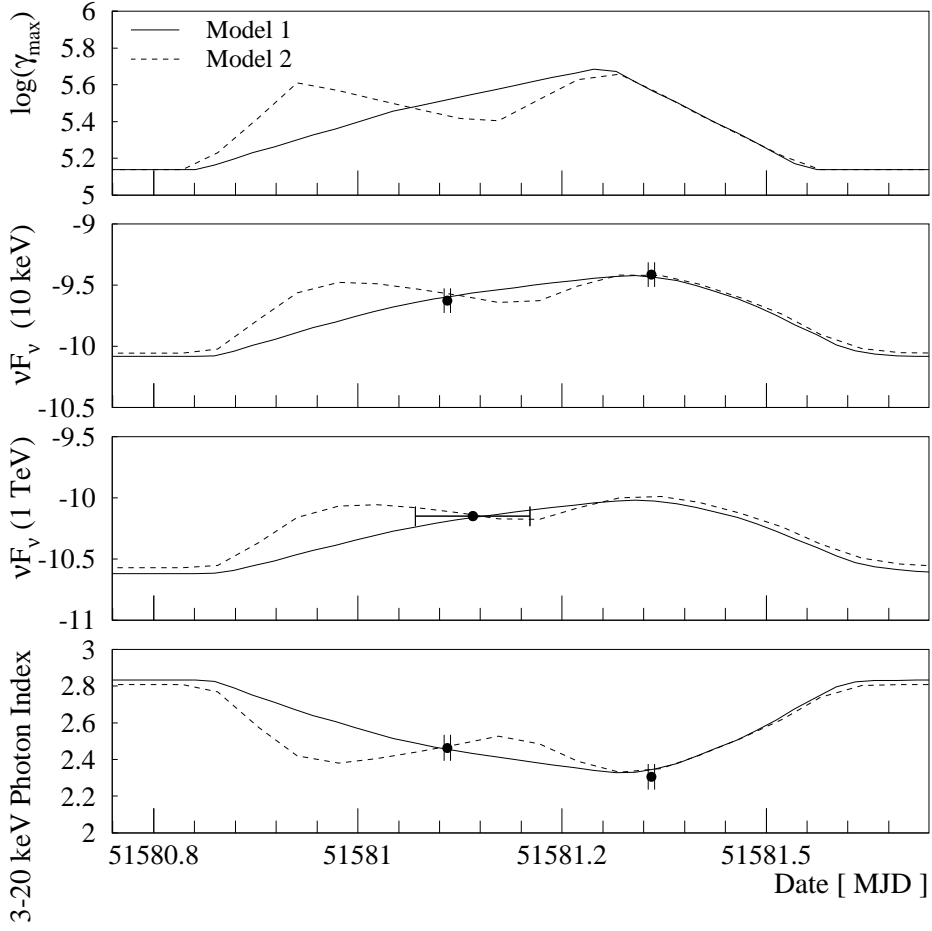


Fig. 4.— From above to below the cut-off electron Lorentz factor, the energy flux at 10 keV, at 1 TeV, and the 3-20 keV photon indices are shown for the data (solid points, horizontal error bars show the length of the observations), and two models (dashed and solid lines). All energy fluxes are in units of 10^{-12} erg cm^{-2} s^{-1} . See text for model parameters and systematic errors on the data points.

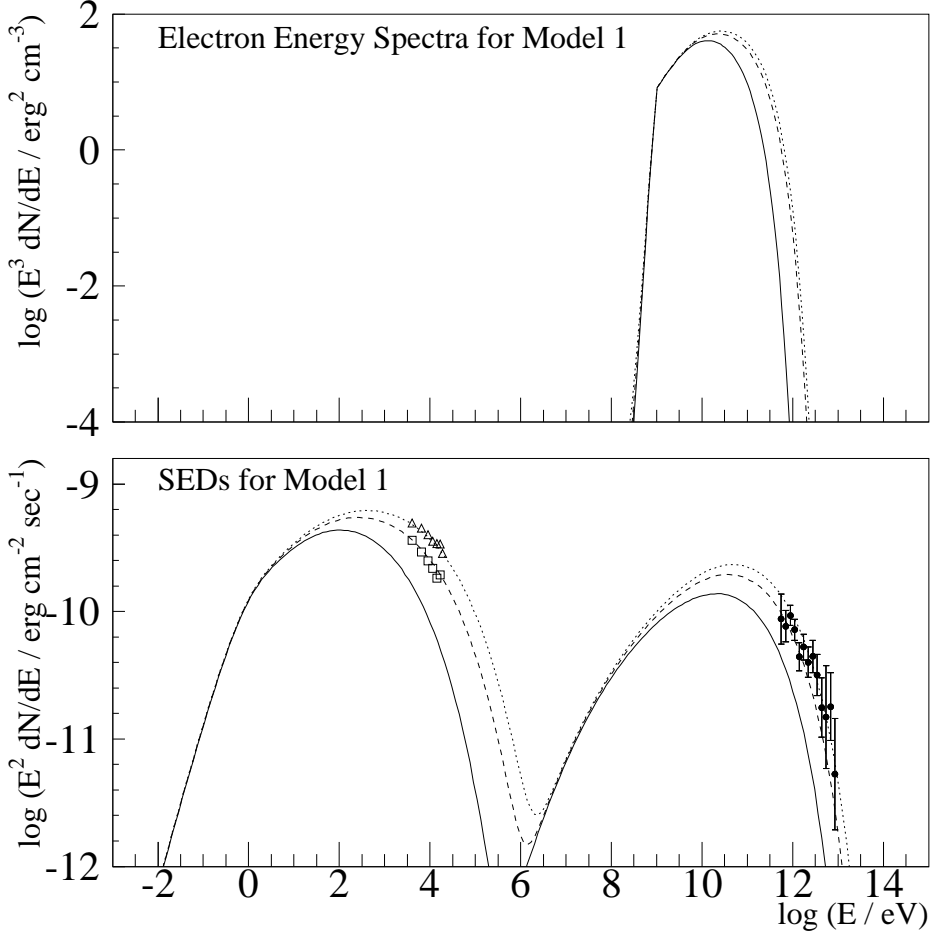


Fig. 5.— The upper panel shows the model estimate for the electron density in the emission region (times the third power of energy), and the lower panel shows the observed (symbols) and modelled (lines) SEDs. The electron energies are given in the jet frame and the photon energies in the observer’s frame. The model estimates correspond to the solid lines of Fig. 4. The squares and the triangles show the *RXTE* spectra measured from 51581.1048-51581.1148 and 51581.3557-51581.3652, respectively. The solid circles show the HEGRA data measured during MJD 51581.0702-51581.2119 which included the first *RXTE* pointing (statistical errors only, see text for systematic errors). The solid, dashed and dotted line show the model of the low-flux spectrum before the flare, and during the first and second *RXTE* pointing, respectively. Note that the model prediction for the HEGRA spectrum is to very good approximation shown by the dashed line.

Table 1. Integral TeV fluxes above 1 TeV
(Statistical errors only - see text for systematic errors)

Start MJD	$t_{\text{obs}}^{\text{a}}$ [hrs]	$N(> 1 \text{ TeV})^{\text{b}}$
51576.1020	1.92	11.02±3.12
51576.2404	0.98	6.08±7.87
51577.0476	4.02	7.34±1.91
51577.0433	0.79	5.89±8.05
51578.1634	1.61	11.24±3.41
51578.2354	0.67	8.64±5.76
51579.0422	4.16	19.29±2.18
51579.0067	1.89	16.90±6.52
51580.0390	3.21	5.50±2.28
51581.0702	3.40	23.96±2.49
51581.2272	1.16	5.12±8.86
51582.0603	3.63	22.79±2.43
51582.2240	1.16	24.81±7.99
51583.0502	3.77	9.50±2.00
51583.2213	1.17	4.34±6.83
51584.0460	3.43	2.43±1.93
51585.0683	3.27	12.70±2.22
51585.2158	1.17	6.98±7.93
51586.0680	0.93	25.32±5.19
51586.2136	1.16	15.21±7.96
51587.0840	2.72	8.22±2.17
51587.2103	1.19	12.31±7.25
51588.1250	1.85	4.75±2.91
51589.1660	0.87	17.20±5.02
51669.9837	0.63	3.41±2.87
51670.8837	2.14	13.33±2.42
51670.9810	1.02	11.03±5.47

^a Net exposure

^b Integral flux above 1 TeV in units
of (10^{-12} photons $\text{cm}^{-2} \text{s}^{-1}$)

Table 2. Results of power-law fits to the 3 keV – 20 keV data (Statistical errors only)

Start MJD	$t_{\text{obs}}^{\text{a}}$ [min]	$F_{3-20\text{keV}}^{\text{b}}$	Γ^{c}	$\chi_{\text{r}}^2 / \text{d.o.f.}^{\text{d}}$	P_{c}^{e}
51579.1485	18.1	385.3 ± 2.1	2.544 ± 0.012	1.22 / 38	0.17
51579.2158	11.7	407.0 ± 2.6	2.527 ± 0.014	1.46 / 38	0.033
51580.5430	52.5	496.9 ± 1.4	2.470 ± 0.006	3.10 / 38	$4.1 \cdot 10^{-10}$
51581.1048	14.4	521.5 ± 3.8	2.469 ± 0.016	1.17 / 38	0.21
51581.3558	13.6	801.9 ± 4.8	2.262 ± 0.012	1.31 / 38	0.097
51582.0812	13.1	402.7 ± 2.0	2.571 ± 0.011	1.18 / 38	0.2
51582.1044	11.7	419.0 ± 2.2	2.588 ± 0.011	1.48 / 38	0.029
51583.0693	24.0	300.2 ± 1.7	2.545 ± 0.012	1.34 / 38	0.077
51584.0736	13.3	140.9 ± 1.7	2.743 ± 0.027	0.84 / 38	0.75
51585.1369	4.0	203.5 ± 2.9	2.746 ± 0.031	0.71 / 38	0.91
51585.2035	14.7	267.9 ± 1.7	2.568 ± 0.013	0.92 / 38	0.61
51586.1333	0.3	460.1 ± 18.8	2.380 ± 0.085	0.78 / 38	0.84
51586.2021	5.3	369.4 ± 3.8	2.450 ± 0.022	0.83 / 38	0.76
51587.1320	0.8	207.9 ± 6.3	2.881 ± 0.072	0.77 / 38	0.84
51587.2017	12.3	154.2 ± 1.7	2.942 ± 0.027	0.58 / 38	0.98
51588.1279	12.8	245.4 ± 2.0	2.748 ± 0.019	0.89 / 38	0.67
51588.1931	21.3	164.8 ± 1.3	2.950 ± 0.019	1.08 / 38	0.34
51589.1891	22.1	172.2 ± 1.4	2.875 ± 0.018	1.16 / 38	0.23
51590.1867	21.9	126.7 ± 1.2	2.909 ± 0.023	1.16 / 38	0.23
51667.0272	24.0	1018.0 ± 1.8	2.195 ± 0.004	4.64 / 38	$9.9 \cdot 10^{-20}$
51667.8838	22.4	506.8 ± 2.1	2.405 ± 0.009	1.16 / 38	0.23
51668.0120	18.1	451.8 ± 2.2	2.435 ± 0.010	0.79 / 38	0.81
51668.8814	24.0	656.7 ± 2.2	2.401 ± 0.007	1.08 / 38	0.34
51668.9321	7.2	511.1 ± 3.6	2.502 ± 0.015	0.89 / 38	0.67
51668.9406	24.8	525.2 ± 2.0	2.495 ± 0.008	1.17 / 38	0.22
51669.9278	49.6	385.1 ± 1.2	2.513 ± 0.007	1.55 / 38	0.016
51670.9250	29.1	368.8 ± 1.1	2.412 ± 0.006	1.72 / 38	0.004
51671.9206	28.5	517.1 ± 1.9	2.396 ± 0.008	2.06 / 38	$1.4 \cdot 10^{-4}$
51672.9231	11.5	664.6 ± 2.7	2.323 ± 0.008	1.65 / 38	0.007

^a Net exposure

^b 3-20 keV flux in units of (10^{-12} ergs cm^{-2} s^{-1})

^c 3-20 keV photon index

^d Reduced χ^2 -value and degrees of freedom of the power-law fit

^e Chance probability for larger reduced χ^2 -values

Table 3. e -folding times of the fastest 3-20 keV flux increases and decreases

MJD1 ^a	MJD2 ^b	Δt ^c [hrs]	τ ^d [hrs]
51585.1369	51585.2035	1.6	5.82 ± 0.32
51586.1333	51586.2021	1.7	-7.54 ± 1.45
51587.1320	51587.2017	1.7	-5.61 ± 0.61
51588.1279	51588.1931	1.6	-4.12 ± 0.12
51668.8814	51668.9321	1.0	-4.32 ± 0.14
51668.8814	51668.9406	1.4	-6.38 ± 0.14

^a Start of first observation

^b Start of second observation

^c Time difference between observations

^d e -folding time

Table 4. Fastest changes of 3-20 keV photon index

MJD1 ^a	MJD2 ^b	Δt ^c [hrs]	$\Delta\Gamma / \Delta t$ ^d [hrs ⁻¹]
51581.1048	51581.3558	6.0	-0.034 ± 0.003
51585.1369	51585.2035	1.6	-0.11 ± 0.02
51586.1333	51587.2017	25.6	0.022 ± 0.003
51588.1279	51588.1931	1.6	0.12 ± 0.02
51668.8814	51668.9321	1.1	0.09 ± 0.02

^a Start of first observation

^b Start of second observation

^c Time difference between observations

^d Change in spectral index per 1 hr, negative values denote spectral hardening

Table 5. Results of power-law fits to the 500 GeV – 5 TeV data (Statistical errors only - see text for systematic errors)

Start MJD	$t_{\text{obs}}^{\text{a}}$ [hrs]	N_0^{b}	Γ^{c}	$\chi_{\text{r}}^2 / \text{d.o.f.}^{\text{d}}$	P_{c}^{e}
51579.0422	4.16	33.51 + 2.76- 3.16	2.76 + 0.16- 0.14	1.42 / 8	0.18
51581.0702	3.40	44.21 + 2.71- 3.37	2.70 + 0.14- 0.10	0.54 / 8	0.83
51582.0603	3.63	36.27 + 2.99- 2.76	2.72 + 0.12- 0.10	3.05 / 8	0.002
51583.0502	3.77	19.63 + 2.92- 3.20	2.98 + 0.34- 0.24	0.87 / 8	0.54
51585.0683	3.27	24.90 + 3.14- 3.22	3.02 + 0.28- 0.24	1.09 / 7	0.47

^a Net exposure

^b Normalization constant in units of (10^{-12} photons $\text{cm}^{-2} \text{s}^{-1} \text{TeV}^{-1}$)

^c Power law photon index

^d Reduced χ^2 -value and degrees of freedom

^e Chance probability for larger reduced χ^2 -values

Table 6. Results of broken power-law fits to the 3 keV – 25 keV data (Statistical errors only)

Start MJD	$t_{\text{obs}}^{\text{a}}$	$k_{1\text{keV}}^{\text{b}}$	E_{b} [keV]	Γ_1^{c}	Γ_2^{d}	$\chi_{\text{r}}^2 / \text{d.o.f.}^{\text{e}}$	P_{c}^{f}
51580.5430	52.5	0.383+0.005-0.006	7.40+0.28-0.32	2.415+0.009-0.010	2.646+0.026-0.027	1.11/46	0.281
51667.0272	24.0	0.456+0.005-0.005	6.96+0.31-0.28	2.137+0.007-0.008	2.301+0.014-0.012	1.19/46	0.173
51670.9250	29.1	0.255+0.005-0.005	6.60+0.81-0.49	2.358+0.015-0.014	2.520+0.034-0.023	0.67/46	0.957
51671.9206	28.5	0.353+0.007-0.008	8.03+1.07-1.03	2.357+0.013-0.017	2.560+0.069-0.053	1.09/46	0.310
51672.9231	11.5	0.385+0.009-0.009	7.46+0.84-0.55	2.268+0.016-0.015	2.477+0.048-0.035	0.75/46	0.897

^a Net exposure in units of (min)

^b Flux at 1 keV in units of (photons keV⁻¹ cm⁻² s⁻¹)

^c Low energy photon index

^d High energy photon index

^e Reduced χ^2 -value and degrees of freedom

^f Chance probability for larger reduced χ^2 -values